frontiers | Frontiers in Molecular Neuroscience

TYPE Original Research
PUBLISHED 27 June 2023
DOI 10.3389/fnmol.2023.1181626

OPEN ACCESS

EDITED BY
Matthias Soller,
University of Birmingham, United Kingdom

REVIEWED BY
Michael R. Ladomery,
University of the West of England,
United Kingdom
Santiago Vernia,
Medical Research Council, United Kingdom

*CORRESPONDENCE
Lucy Donaldson
✉ Lucy.Donaldson@nottingham.ac.uk
David O. Bates
✉ David.Bates@nottingham.ac.uk

RECEIVED 07 March 2023
ACCEPTED 16 May 2023
PUBLISHED 27 June 2023

CITATION
Alalwany RH, Hawtrey T, Morgan K, Morris JC, Donaldson LF and Bates DO (2023) Vascular endothelial growth factor isoforms differentially protect neurons against neurotoxic events associated with Alzheimer's disease. *Front. Mol. Neurosci.* 16:1181626. doi: 10.3389/fnmol.2023.1181626

Vascular endothelial growth factor isoforms differentially protect neurons against neurotoxic events associated with Alzheimer's disease

Roaa H. Alalwany[1], Tom Hawtrey[2], Kevin Morgan[3], Jonathan C. Morris[2], Lucy F. Donaldson[3]* and David O. Bates[1,4]*

[1]Tumour and Vascular Biology Laboratories, Division of Cancer and Stem Cells, Centre for Cancer Sciences, School of Medicine, Biodiscovery Institute, University of Nottingham, Nottingham, United Kingdom, [2]School of Chemistry, University of New South Wales, Sydney, NSW, Australia, [3]School of Life Sciences, University of Nottingham, Nottingham, United Kingdom, [4]Pan African Cancer Research Institute, University of Pretoria, Pretoria, South Africa

Alzheimer's disease (AD) is the most common cause of dementia, the chronic and progressive deterioration of memory and cognitive abilities. AD can be pathologically characterised by neuritic plaques and neurofibrillary tangles, formed by the aberrant aggregation of β-amyloid and tau proteins, respectively. We tested the hypothesis that VEGF isoforms VEGF-A_{165}a and VEGF-A_{165}b, produced by differential splice site selection in exon 8, could differentially protect neurons from neurotoxicities induced by β-amyloid and tau proteins, and that controlling expression of splicing factor kinase activity could have protective effects on AD-related neurotoxicity *in vitro*. Using oxidative stress, β-amyloid, and tau hyperphosphorylation models, we investigated the effect of VEGF-A splicing isoforms, previously established to be neurotrophic agents, as well as small molecule kinase inhibitors, which selectively inhibit SRPK1, the major regulator of VEGF splicing. While both VEGF-A_{165}a and VEGF-A_{165}b isoforms were protective against AD-related neurotoxicity, measured by increased metabolic activity and neurite outgrowth, VEGF-A_{165}a was able to enhance neurite outgrowth but VEGF-A_{165}b did not. In contrast, VEGF-A_{165}b was more effective than VEGF-A_{165}a in preventing neurite "dieback" in a tau hyperphosphorylation model. SRPK1 inhibition was found to significantly protect against neurite "dieback" through shifting AS of *VEGFA* towards the VEGF-A_{165}b isoform. These results indicate that controlling the activities of the two different isoforms could have therapeutic potential in Alzheimer's disease, but their effect may depend on the predominant mechanism of the neurotoxicity—tau or β-amyloid.

KEYWORDS

Alzheimer's disease, VEGF, splicing, tau, SRPK1, amyloid-beta

1. Introduction

The neurovascular unit (NVU) controls blood–brain barrier (BBB) permeability and cerebral blood flow, maintaining the chemical composition of cerebral tissue required for its proper function (Zlokovic, 2011). The NVU unit comprises vascular cells (endothelium, pericytes and smooth muscle), glial cells and neurones. Dysfunction of the NVU, and resulting

disruption to the BBB, is associated with the accumulation of neurotoxins, including β-amyloid, as well as a reduction in cerebral blood flow and hypoxia. Cerebrovascular deficits are common in AD: >50% of patients have ischaemic white matter damage and > 90% of patients have cerebral amyloid angiopathy, characterised by the deposition of β-amyloid in vessel walls (Thomas et al., 2015). Furthermore, vascular risk factors, such as atherosclerosis and diabetes mellitus, also increase risk of developing AD (Yang et al., 2004).

There is growing evidence that amyloid production and cerebral hypoperfusion are inherently linked to each other in AD pathology. VEGF-A, a key regulator of angiogenesis, is known to bind to amyloid peptides with high affinity (50 pM; Yang et al., 2004) and specificity. In addition, it has been found to co-localise with amyloid plaques in the AD brain (Yang et al., 2004). β-amyloid treatment has been shown to alter angiogenesis in a concentration dependent manner: At lower concentrations, amyloid can result in the stimulation of microvessel formation whereas higher concentrations significantly inhibit the angiogenic process in endothelial cells (Paris et al., 2004). Investigation of amyloid's anti-angiogenic activity found that it can inhibit VEGFR2 activation by directly binding and acting as an antagonist of the receptor (Patel et al., 2010). Furthermore, β-amyloid treatment of endothelial cells can reverse a VEGF-A induced increase in permeability. Considering VEGF-A is a very potent permeability factor, these studies put forward evidence of amyloid's ability to antagonise VEGF-A related activity.

Interestingly, levels of VEGF-A are increased in the AD brain, specifically in the frontal cortex and para-hippocampus (Thomas et al., 2015). In addition, the total level of VEGFR1, a negative regulator of VEGF-A expression, is reduced in AD despite being upregulated by hypoxia (Harris et al., 2018). However, this may be offset by the fact the ratio of membrane bound to soluble VEGFR1 is also reduced, since soluble VEGFR1 is thought to be signalling inactive and can sequester VEGF-A by acting as a competitive inhibitor of its ligand. Ultimately, this suggests that inhibition of VEGF-A binding at VEGFR2, and related VEGF-A mediated activity, may be driving upregulation of its expression. Indeed, Thomas et al. (2015) suggested that overproduction of VEGF-A in AD may be a compensatory mechanism for reduced cerebral perfusion associated with the accumulation of amyloid. This is supported by evidence that VEGF-A expression positively correlates with disease severity (Thomas et al., 2015). Since cerebral hypoperfusion persists as a symptom of AD, endogenous upregulation of VEGF-A may be an insufficient response to NVU dysfunction. Exogenous VEGF-A can oppose the effect of high amyloid concentrations and partially restore angiogenic activity *in vitro* (Patel et al., 2010) suggesting that stimulation of VEGF-A activity could be relevant to neuroprotection. However, it is important to elucidate the direct effect on neurones as the majority of studies so far have only characterised role of VEGF-A in the endothelial cell component of the NVU.

As a hallmark of AD pathology, neurofibrillary tangles (NFTs) are the second key driver of cognitive decline. NFTs are mainly comprised of hyperphosphorylated tau, a protein particularly abundant in neurones, and lead to cell dysfunction and death (Theofilas et al., 2018). Compared with amyloid, there is less published evidence linking NFTs to VEGF-A biology. Nonetheless, diminished VEGF-A has been correlated with the presence of NFTs in AD cortices (Provias and Jeynes, 2008). Furthermore, the ratio of phosphorylated tau to amyloid is considered a strong positive predictor of cognitive decline and has been used to identify other CSF biomarkers for AD (Harari et al., 2014). A mouse model study demonstrated that lentiviral VEGF-A treatment can reverse AD-related increase in hyperphosphorylated tau as well as amyloid accumulation (Salomon-Zimri et al., 2016). Considering this evidence of crosstalk between amyloid, tau and VEGF-A, it is necessary to account for both amyloid and tau hypotheses in order to properly understand the role of VEGF-A in AD pathology.

It is increasingly clear that VEGF-A is not limited to its original discovery as a vascular protein but rather a pleiotropic protein that exerts cytoprotective effects in the nervous system (Greenberg and Jin, 2005) and the two families of isoforms—the VEGF-A_{165}a and VEGF-A_{165}b families (Harper and Bates, 2008) have different functions—while both can be neuroprotective (Beazley-Long et al., 2013), VEGF-A_{165}b is not angiogenic and can block blood vessel growth induced by VEGF-A_{165}a (Harper and Bates, 2008). It has thus been proposed that the VEGF-A_{165}b isoforms act as homeostatic growth factors, whereas the VEGF-A_{165}a are remodelling factors. As such VEGF isoforms have been proposed to act as a neuroprotective agent implicated in a number of neurodegenerative conditions, including AD (Storkebaum et al., 2004). In cases of ischemic injury, VEGF-A not only protects neural tissue by reperfusion but also directly exerts neurotrophic (survival) and neurotropic (neurogenesis) actions (Hobson et al., 2000). We therefore investigated the use of VEGF-A as a neuroprotective agent using *in vitro* models relevant to AD pathology. In addition, we aimed to look at the effects of the alternatively spliced isoform VEGF-A_{165}b, which has previously been shown to protect against sensory neuronal degeneration in a model of diabetes (Hulse et al., 2015) but has not yet been studied in AD. The SRPK1 inhibitor Sphinx31, which can shift VEGF-A splicing from VEGF-A_{165}a to VEGF-A_{165}b isoforms, has never been used in the context of AD either. We initially established a neuronal cell assay based on oxidative stress since ROS production is widely accepted to be crucial to amyloid plaque toxicity (Cheignon et al., 2018), and then proceeded to use amyloid as a direct neurotoxin. Finally, we investigated the effect of VEGF-A and Sphinx31 treatments in an assay based on the induction of tau hyperphosphorylation (Metin-Armagan et al., 2018).

2. Materials and methods

2.1. Cell culture and cell differentiation

Unless otherwise stated, all cell culture reagents were purchased from Thermo Fisher Scientific. All cell culture was performed in cell culture hoods in class II facilities using aseptic technique and sterile culture medium. Cell culture flasks were kept in an incubator at 37°C in a humidified environment containing 5% CO_2. SHSY5Y cells were cultured in DMEM/F-12 GlutaMAX media with 10% Foetal Bovine Serum (FBS); Neuro2a cells were cultured in RPMI media + 2 mM L-glutamine + 10% FBS.

Prior to treatment. SH-SY5Y cells were differentiated by reduction to 1% serum and treatment with 10 μM all-trans retinoic acid for 7 days. Differentiation media was renewed at least every 3 days. Neuro2a cells were differentiated by serum starvation and treatment with 300 μM dibutyryl cAMP for 48 h.

2.2. Cell viability assay

All cell viability assays were carried out on SHSY5Y cells and Neuro2a cells seeded in black-sided flat clear bottom 96-well plates. After differentiation and treatment, 10 µL WST-1 reagent was added to 100 µL media alone or cells with 100 µL treatment media. After 1 h, 2 h and (only if necessary) 4 h, plates were read at 450 nm with a reference wavelength of 620 nm. Incubations were performed under normal sterile cell culture conditions, at 37°C in a humidified environment containing 5% CO_2. Readings from treated cells were normalised against an assay control (media + WST-1 reagent) and the relevant experimental control (e.g., vehicle only). Cells were treated with neurotoxic agents hydrogen peroxide, β-amyloid or okadaic acid for 24 h with and without 2.5 nM VEGF-A co-treatment. Neuroprotective agent NGF was used as a positive control. For SRPK1 inhibition, cells were treated with Sphinx31, synthesised as described by Batson et al. (2017) for 24–72 h (depending on assay) at a range of 1–10 µM.

2.3. Immunofluorescence

SHSY5Y cells were fixed in black-sided flat clear bottom 96-well plates with 4% PFA for 10 min at RT (50 µL per well). Fixed cells were washed once with 200 µL PBS and then permeabilised with 100 µL PBS 0.2% Triton X100 (PBSX) with 1% normal horse serum for 30 min. A mouse anti-human βIII tubulin antibody (R&D Systems) was used as a marker of neurite outgrowth. It was diluted 1:1,000 in 1% normal horse serum PBS and 50 µL was added to each well after cell permeabilisation, then incubated (in a humid box) overnight at 4°C. The following day, wells were washed three times for 5 min each with 200 µL PBS 0.5 mL/L Tween20. Donkey anti-mouse Alexafluor-488 secondary antibody and Hoechst were diluted 1:1,000 in 1% BSA PBS and 50 µL added to each well. Cells were incubated for 30 min in the dark at RT, and cells were washed again three times with 200 µL PBS 0.5 mL/L Tween20. Cells were kept in 100 µL PBS at 4°C until imaged. Fluorescence was captured using a Leica SPE confocal microscope: three 20x images were taken per well with smart gain of 700 or 800 (always kept consistent across experimental groups). There were 4–6 wells per condition in each experiment, making a total of 12–18 images per condition. Images were analysed on Image J using simple neurite tracer. The sum length of neurites per image was normalised to the number of cells, automatically calculated with a mask of Hoechst-stained nuclei. Average neurite length was then compared between treatment groups.

2.4. RNA extraction and amplification

2.4.1. RNA extraction

RNA was extracted from cells after differentiation and treatment using a TRI-reagent protocol. Firstly, media was removed from cells and 500 µL TRI-reagent was added directly to culture dish. The cell lysate was homogenised with a pipette before transfer to an Eppendorf tube. After 5 min incubation at RT, 250 µL chloroform was added and samples were shaken vigorously by hand for 1 min, then left to incubate for 10 min at RT. Samples were centrifuged at 12,000 × *g* for 15 min at 4°C for phase separation: a red organic phase (containing protein), an interphase (containing DNA) and a colourless aqueous phase (containing RNA). The top aqueous phase was transferred into an ice-chilled Eppendorf tube with equal-volume isopropanol. Samples were shaken for 15 s and RNA was allowed to precipitate overnight at −20°C. Next, samples were centrifuged at 12,000 × *g* for 15 min at 4°C to pellet the RNA. The supernatant was discarded, and the RNA pellet was washed with 1 mL 75% ethanol and re-pelleted by centrifugation at 7,500 × *g* for 15 min at 4°C. The supernatant was discarded, and the RNA pellet was allowed to air-dry before being resuspended in 10–30 µL sterile water. RNA was kept on ice for 30 min before being quantified using a spectrophotometer (Thermo-Scientific Nanodrop 2000) and stored at −80°C.

2.4.2. cDNA generation

RNA was reverse transcribed to complementary DNA (cDNA) using the Takara PrimeScript™ RT Reagent Kit (RR037A). For each sample, 1 µg RNA was combined with 25 pM oligo dT, 200 pM random hexamers and PrimeScript buffer, then made up to a reaction volume of 19 µL with sterile water. The reaction mixtures were heated to 65°C for 10 min for denaturation and then immediately placed on ice for the addition of 1 µL PrimeScript RT enzyme. Following this, reaction mixtures were incubated at 25°C for 10 min and 37°C for 60 min for generation of 50 ng cDNA. RT enzyme was inactivated by heating to 85°C for 1 min and cDNA samples were stored at -20°C. For each experiment, a no-template control was run to check for contamination, including all components of the reaction mixture excluding the RNA sample.

2.4.3. Polymerase chain reaction

All PCR reactions were performed on 50 ng cDNA using GoTaq G2 Green Master Mix (Promega) at a total volume of either 15 or 30 µL. Primers were used at a final concentration of 0.4 µM. DNA samples were denatured at 96°C for 5 min, followed by multiple cycles of denaturation at 96°C for 30 s, annealing at primer specific temperature at 55°C for 30 s, and extension at 72°C for 1 min. PCR cycles were followed by a final extension step at 72°C for 10 min and samples were then held at 4°C until gel electrophoresis. PCR products were run in 2% agarose gels containing 50 ng/mL ethidium bromide at 100 V for approximately 1.5 h. Gels were visualised using the BioRad Gel Doc™ EZ System. Primers used were as follows: MAPT: Forward: 5′-CTCCAAAATCAGGGGATCGC-3′, Reverse 5′-CCTTGCTCAGG TCAACTGGT-3′. GAPDH Forward 5′-AATTC CATGGCACCGT CAAG-3′. Reverse 5′-GGTCATGAGTCCTTCCACGA-3′.

2.5. Protein extraction and assays

2.5.1. Cell lysis

Protein was extracted from cells after differentiation and treatment. Cells were washed with ice-cold PBS and kept on ice. Cell lysis buffer (NP40, 1X, PMSF, 1 mM, Na_3VO_4, 10 mM, NaF, 5–50 mM Protease Inhibitor, 1X Roche complete cocktail) was added to cells and left to incubate for 10 min. Cells adhered to the surface of culture plates were scraped and mechanically dissociated by trituration, and then transferred to an ice-chilled Eppendorf. The cell suspension was vortexed for 15 s three times over a 10 min incubation on ice. Samples

were centrifuged at 12,000 × g for 10 min at 4°C and the supernatant was collected in a fresh Eppendorf and stored at −80°C.

2.5.2. Protein quantification

A Bradford protein reagent assay (Bio-Rad) was used to quantify the protein concentration of samples against a seven-point standard curve of bovine serum albumin (BSA) in PBS (1,000 µg/mL serially diluted 1:1 to 15.625 µg/mL). Samples were diluted 1:10 or 1:20 in PBS to bring them within range of the standard curve. 10 µL of standards and samples were loaded in triplicate into a clear 96 well plate. Bradford reagent was diluted 1:5 in distilled water and 200 µL was loaded to each well. Plates were agitated for 5 s and then read immediately at 620 nm using a Magellan microplate reader. A standard curve was plotted on Microsoft Excel using optical density readings from the BSA standards, and sample protein concentrations were calculated based on the equation of the curve.

2.5.3. ELISA

An antibody selective for the VEGF-A_{165}a isoform was generated by BioRad HuCAL technology using a peptide corresponding to the c terminus of VEGF-A_{165}a (TCRCDKPRR). High-binding 96-well clear microplates were coated with 100 µL capture antibody at 075 µg/mL (anti-VEGF-A_{165}a) or 10 µg/mL (anti-VEGF-A_{165}b, MRVL56/1, Abcam), sealed with parafilm and incubated (with agitation) overnight at RT. The following day, wells were washed three times with wash buffer (PBS + 0.05% Tween20). After each wash, plates were inverted and firmly tapped on tissue paper to completely empty wells and prevent carry-over of liquid or bubbles. 100 µL blocking buffer [PBS + 1% BSA (sterile-filtered) or SuperBlock (ThermoFisher)] was added to coated plates, sealed with parafilm, and incubated (with agitation) for 2 h at RT. After block, wells were washed again (as before) and 100 µL standards or samples were added in duplicate according to plate layout planned for the experiment. VEGF-A_{165}a and VEGF-A_{165}b recombinant proteins were used as standards, starting at 1000 pg./mL and serially diluted 1:1 in diluent to a low concentration of 3.9 pg./mL, making a nine-point standard curve. The opposite VEGF-A isoform was used at highest concentration as a negative control to ensure specificity of the capture antibody. Samples were typically diluted 1 in 2, also using diluent [PBS + 1% BSA (sterile-filtered)]. After addition of standards and samples, plate was resealed with parafilm and incubated (with agitation) for 2 h at RT. As detection antibody, 100 µL biotinylated mouse monoclonal anti-human VEGF-A antibody (BAF293, R&D Systems) was added to each well following another set of washes. Plates were resealed and incubated (with agitation) for another 2 h at RT. Plates were washed (as before) and 100 µL horseradish peroxidase conjugated streptavidin (made up in diluent) was then added to each well. Plates were sealed with foil to protect from light and incubated for 30 min at RT. Plates were washed a final time and 100 µL tetramethylbenzidine (TMB) substrate was added to each well, then incubated in the dark for 1 h (or until the colour change reached an appropriate intensity) at RT. The reaction was quenched with 50 µL 1 M HCL per well and shaking for 10 s to ensure thorough mixing. Finally, plates were read at 450 nm using a Magellan microplate reader. A standard curve was plotted on Microsoft Excel using optical density readings from the VEGF-A standards, and sample concentrations for VEGF-A isoforms were calculated based on the equation of the curve.

2.6. Statistical analysis

Statistics were performed in Graphpad Prism. Curve fitting was undertaken with a four variable curve fit. Statistical tests were undertaken as described in the figures. *Post hoc* analysis was undertaken for one-way ANOVA using Holm-Sidak tests. Values are given as mean ± standard error of the mean unless otherwise stated. Ratios of VEGF-A_{165}a to VEGF-A_{165}b were calculated as the concentration of VEGF-A_{165}a to that of VEGF-A_{165}b.

3. Results

3.1. VEGF-A isoforms are neuroprotective against oxidative stress

To establish an assay of neuronal toxicity, SHSY5Y and N2a cells were treated with hydrogen peroxide, a strong reactive oxygen species that can induce oxidative stress *in vitro* (Bonello et al., 2007) and has been shown in other cell types to be modified by VEGF isoforms, and therefore serves as a good positive control (Beazley-Long et al., 2013). The WST-1 assay showed a decreased cell viability at 150–250 µM in SHSY5Y cells (Figure 1A) and 25–100 µM H_2O_2 in N2a cells (Figure 1B). Co-treatment with the neuroprotective agent NGF was used as a positive assay control since it is known to consistently increase neuronal cell survival (Bogetti et al., 2018). In the WST-1 assay, NGF resulted in a significant increase in viability of both cell lines (two-way ANOVA, $p < 0.01$ and $p < 0.0001$ respectively), validating the use of the assay to investigate the effect of VEGF-A isoforms in this *in vitro* model of oxidative stress. In SHSY5Y cells, treatment with 2.5 nM recombinant VEGF-A_{165}a or VEGF-A_{165}b significantly increased cell viability (two-way ANOVA, $p < 0.01$) in a similar manner to NGF (Figure 1A). There was an upward shift in cell metabolic activity where the drop in the control group induced by 150 µM H_2O_2 (62 ± 9.8% of control) was completely recovered by VEGF-A_{165}a (103 ± 7.5% of no H_2O_2) and VEGF-A_{165}b (93.8 ± 2.5, shown in Figure 1A). In N2a cells, there was no significant difference in the viability with VEGF-A treatment of either isoform (see Figure 1B).

3.2. VEGF-A isoforms are neuroprotective against Aβ-induced neurotoxicity

To model amyloid cytotoxicity in AD, Aβ peptide treatment was used to reduce cell viability in accordance to guidance from previously published methods to prepare amyloid in unaggregated, oligomeric and fibrillar states (Stine et al., 2011). Since amyloid has a tendency to aggregate *in vitro* and its unaggregated form had been shown to reduce viability of N2a cells, this method was selected. In SHSY5Y cells 1 µM amyloid significantly decreased viability to 55% of control after 24 h (Figure 2A). Since 48 h treatment produced a very similar response, the remainder of

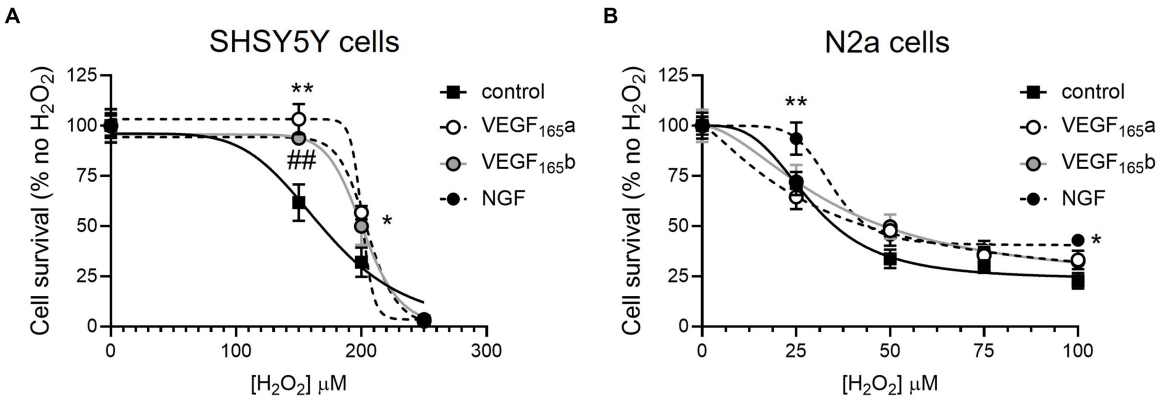

FIGURE 1
VEGF-A isoforms increase metabolic activity of SHSY5Y cells but not N2a cells co-treated with hydrogen peroxide. SHSY5Y cells and N2a cells were treated with H_2O_2 alone or with NGF or 2.5nM VEGF-A isoforms for 24h, and a WST-1 assay was performed to measure metabolic activity. Readings were normalized against an assay control (media+WST-1 reagent) and experimental control (cells treated with PBS or NGF alone+WST-1 reagent). **(A)** Concentration-dependent decrease in percent metabolic activity of SHSY5Y cells with H_2O_2 without (control) or with NGF, VEGF-A_{165}a, or VEGF-A_{165}b (two-way ANOVA, $p<0.01$). **(B)** Concentration-dependent decrease in percent metabolic activity of N2a cells with H_2O_2 without (control) or with NGF, VEGF-A_{165}a, or VEGF-A_{165}b (two-way ANOVA, $p<0.0001$). $N=8$ or $N=12$ readings. *VEGF-A_{165}a different from control; $^{\#\#}$VEGF-A_{165}b different from control; and *NGF different from control. *$p<0.05$, $^{\#\#}$.**$p<0.01$, compared with control, Holm Sidak *post hoc* tests. $N=12$ per group per concentration.

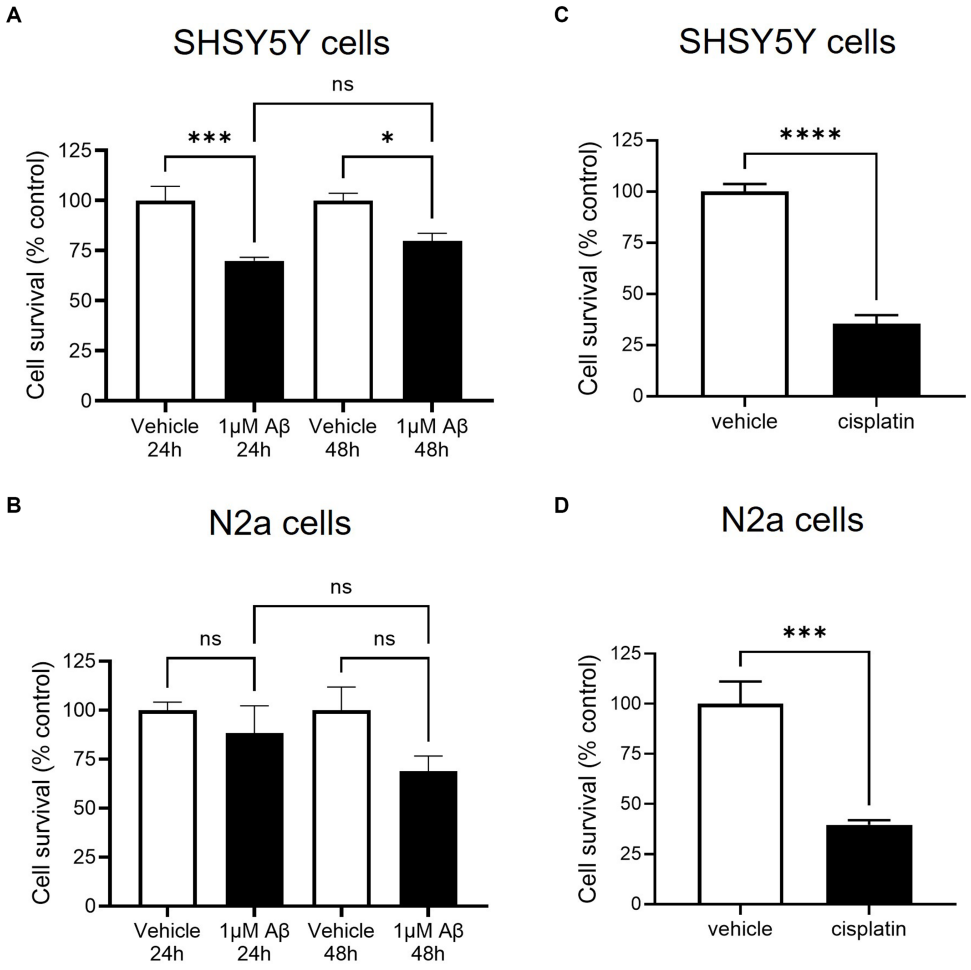

FIGURE 2
β-amyloid (Aβ) decreased cell survival as measured by metabolic activity of SHSY5Y cells but not in N2a cells. SHSY5Y cells and N2a cells were treated with 1 μM Aβ for 24 and 48 h. WST-1 assay was performed to measure metabolic activity and readings were normalised against an assay control (media + WST-1 reagent) and experimental control (cells treated with vehicle alone + WST-1 reagent). $N=6$ readings. **(A)** After both 24 and 48h treatment, SHSY5Y cell metabolic activity was significantly decreased with 1μM Aβ (one-way ANOVA, $p<0.001$). **(B)** N2a cells had a variable response to Aβ; metabolic activity was reduced but not to a significant degree (one-way ANOVA, $p>0.05$). **(C,D)** To confirm the assay worked, cisplatin treatment was shown to decrease metabolic activity in both SHSY5Y cells and N2a cells. ns, not significant; *$p<0.05$, ***$p<0.001$; ****$p<0.0001$ compared with vehicle, Holm Sidak *post hoc* test.

assays were carried out after 24 h incubation. The same optimisation was repeated in N2a cells: although viability decreased to 69 ± 8% of control after 48 h 1 μM amyloid treatment, the assay did not produce a statistically significant decrease in viability (see Figure 2B). To validate the use of WST-1 as a measure of cell viability, both SHSY5Y and N2a cells were treated with a positive control chemotherapy agent cisplatin: 24 h treatment produced a decrease to 35 ± 4 and 40% ±2% of control viability, shown in Figures 2C,D, respectively.

In this model, SHSY5Y cells were treated with recombinant VEGF-A_{165}a and VEGF-A_{165}b to identify whether they could rescue amyloid-related decrease in cell viability. Treatment with 1 μM amyloid alone significantly decreased cell viability, but when co-treated with either VEGF-A_{165}a (in Figure 3A) or VEGF-A_{165}b (in Figure 3B), cell viability returned towards control levels.

3.3. VEGF-A isoforms are neuroprotective against tau hyperphosphorylation induced cytoskeletal destabilisation

To model tau hyperphosphorylation toxicity in AD, neurite outgrowth was selected as a basic measure of neuronal viability and function. This assay is closely related to the primary role of tau as a microtubule-associated protein. Tau stabilises the neuronal cytoskeleton by copolymerising with tubulin for microtubule formation. However, an increase in its phosphorylation reduces its interaction with microtubules, causing destabilisation of the cytoskeleton and neurodegeneration (Lindwall and Cole, 1984; Iqbal et al., 2010). βIII tubulin antibody was selected as a neuronal specific marker (Draberova et al., 1998) and used to probe SHSY5Y cells treated with increasing concentrations of okadaic acid (OA), as presented in Figure 4A. OA was used a neurotoxic agent which induces hyperphosphorlyation of tau (Martin et al., 2011). Quantification showed a concentration-dependent decrease in cell number (Figure 4B) and normalised neurite outgrowth length (Figure 4C). At 3 nM OA, SHSY5Y cells decreased to 60 ± 9% of control cell number and 56 ± 9% of control neurite outgrowth length.

SHSY5Y cells co-treated with OA and recombinant VEGF-A_{165}a (as shown in the second panel of Figure 5A) had significantly increased neurite outgrowth compared with vehicle and with OA alone (two-way ANOVA, $p < 0.0001$). There is an upward shift in neurite length, where in the absence of OA, the average neurite length per cell increased from 22 ± 1 to 30 ± 2 μm (see Figure 5B). With up to 3 nM OA, VEGF-A_{165}a maintained higher neurite outgrowth in SHSY5Y cells, as seen by the increase from 12 ± 1 to 18 ± 1 μm. When neurite outgrowth was normalised to the -OA control in each group, there was overlap between two curves with and without VEGF-A_{165}a (see Figure 5C), indicating that VEGF-A_{165}a increased baseline neurite outgrowth but did not counteract the OA-induced decrease. For example, with 3 nM OA, PBS and VEGF-A_{165}a treated cells had an average 56 ± 5 and 59 ± 3% of their -OA controls, respectively.

In comparison, recombinant VEGF-A_{165}b alone did not induce an increase in neurite outgrowth in vehicle treated SHSY5Y cells (as shown in the second panel of Figure 5A). However, VEGF-A_{165}b treated SHSY5Y cells did maintain significantly higher sum neurite outgrowth when treated with OA (two-way ANOVA, $p < 0.0001$). While 3 nM OA decreased neurite outgrowth from 22 ± 1 to 12 ± 1 μm in the control group, VEGF-A_{165}b treated cells had average neurite length of 22 ± 2 and 21 ± 1 μm, respectively (see Figure 5B). Maintaining similar neurite outgrowth by VEGF-A_{165}b treatment resulted in a rightward shift in the normalised curve, as shown in Figure 5C.

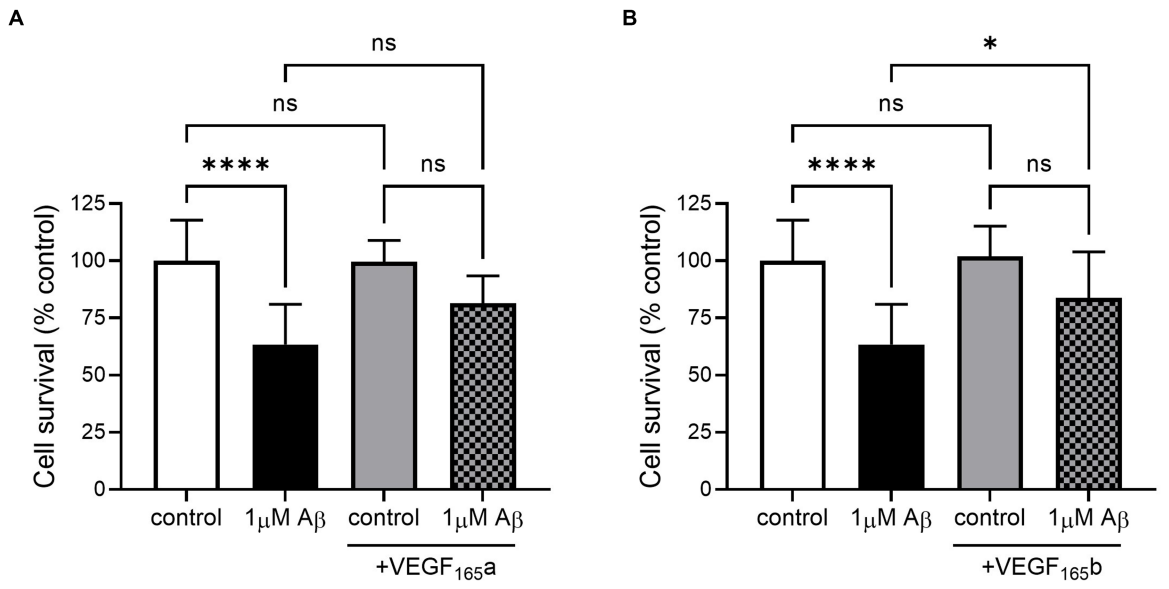

FIGURE 3
VEGF-A_{165}a or VEGF-A_{165}b treatment recovers Aβ-induced decrease in metabolic activity in SHSY5Y cells. **(A)** Normalised metabolic activity showed decrease with 1μM Aβ (one-way ANOVA, $p<0.0001$) and was recovered with co-treatment of 2.5nM VEGF-A_{165}a. Treatment with 2.5nM VEGF-A_{165}a alone did not significantly change metabolic activity. **(B)** Similarly, 2.5nM VEGF-A_{165}b alone did not change metabolic activity but protected against Aβ-induced reduction. $N=4–6$. *$p<0.05$, ****$p<0.0001$ compared with vehicle, Holm Sidak *post hoc* tests.

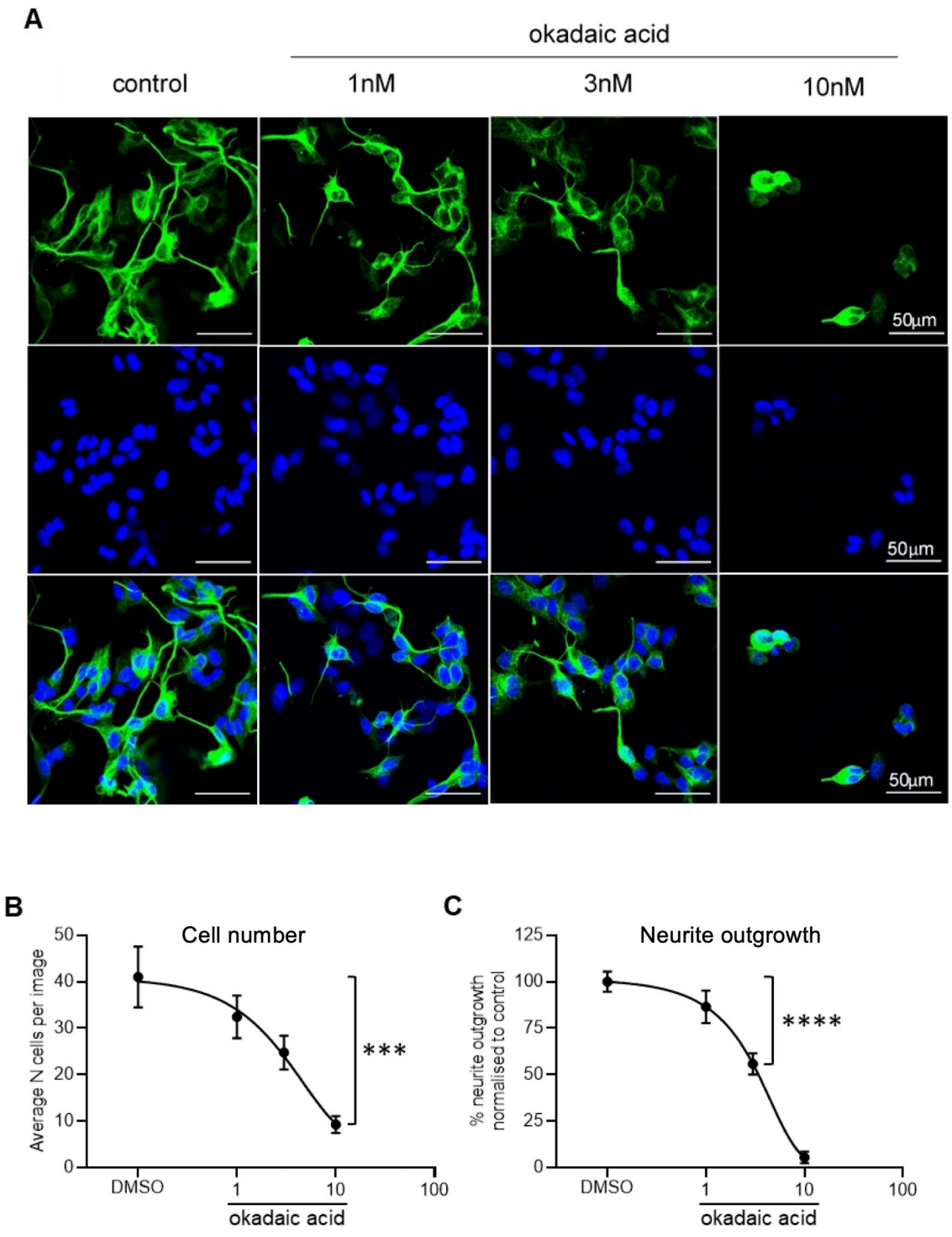

FIGURE 4
Reduced neurite outgrowth with increased concentration of OA. **(A)** Neuron-specific marker βIII tubulin identified neurites in SHSY5Y cells shown in green. Cell nuclei stained with Hoechst shown in blue. Merged images in final row. *N*=18 images per condition. **(B)** Decreased number of live cells with increased concentration of OA. Nuclei automatically counted on FIJI software with a macro. **(C)** Neurite length was quantified using simple tracer and the sum neurite length was divided by number of nuclei. The outgrowth in SHSY5Y cells treated with OA was plotted as percentage of DMSO control. Points=mean, error bars=SEM. ****p<0.0001 compared with vehicle. One way ANOVA with Holm Sidak *post hoc* tests. *N*=3 with six images analysed per repeat.

To quantify the effect of VEGF-A isoforms on OA-induced neurite "dieback," the half maximal inhibitory concentration (IC_{50}) of OA on sum outgrowth (per cell) was compared between groups co-treated with vehicle only, VEGF-A_{165}a or VEGF-A_{165}b (Table 1). VEGF-A_{165}a treatment caused a modest increase in IC_{50} from 3.0 to 3.4 µM whilst VEGF-A_{165}b treatment caused a greater increase to 5.1 µM. This suggests

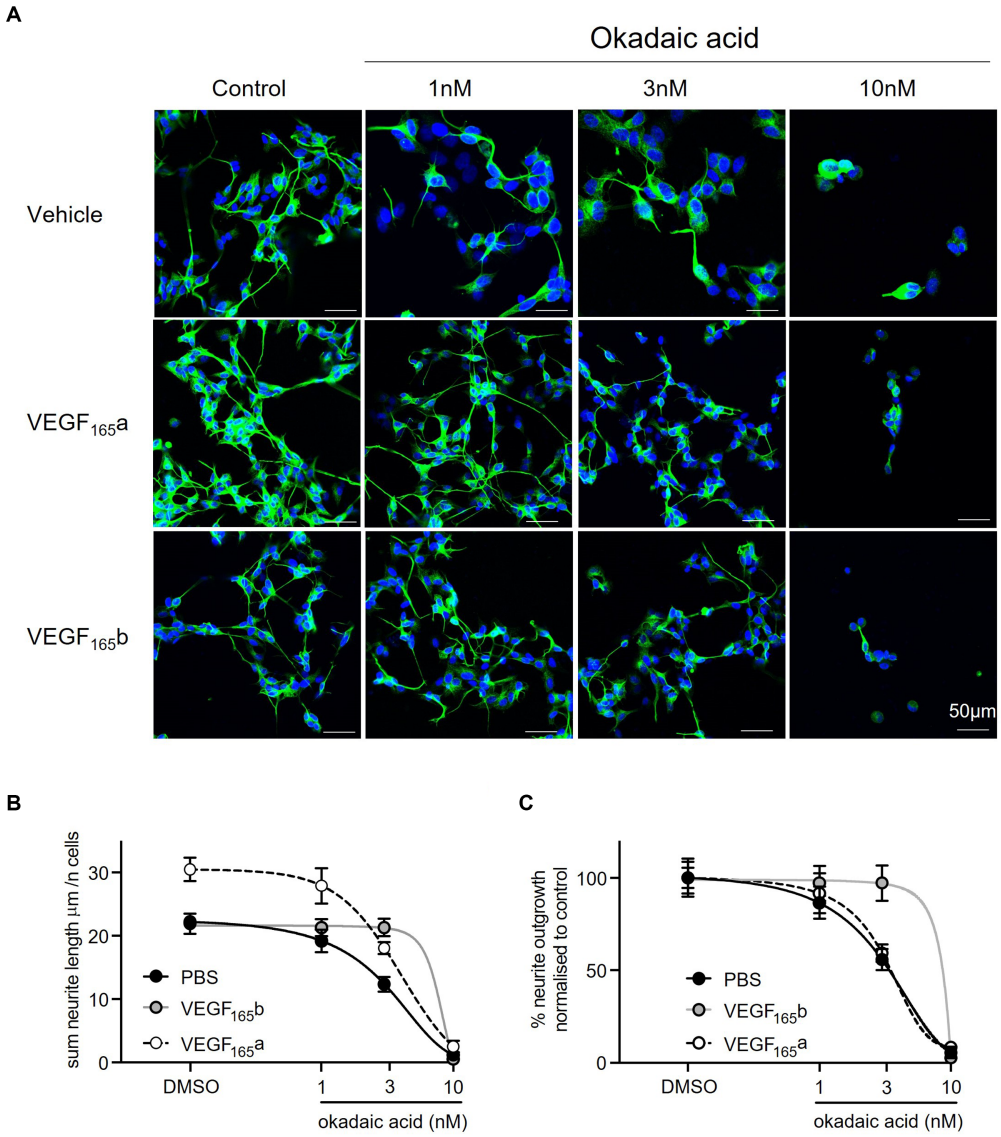

FIGURE 5
VEGF-A_{165}a increased neurite outgrowth in SHSY5Y cells co-treated with OA. **(A)** neuron-specific marker βIII tubulin identified neurites in green. Cell nuclei stained with Hoechst shown in blue. *N*=18 images per condition. **(B)** Using FIJI software, neurite length was quantified using simple tracer, and the sum neurite length was divided by number of nuclei counted with a macro. Plot showed that average neurite length is significantly and consistently higher with VEGF-A_{165} in control, 1 and 3nM OA treatments (two-way ANOVA, $p<0.0001$). With 10nM OA, VEGF-A_{165} did not have an effect. By itself, VEGF-A_{165}b did not increase average neurite length but maintained outgrowth in SHSY5Y cells co-treated with 1 and 3nM OA where average length was significantly higher than PBS control (two-way ANOVA, $p<0.0001$). With 10nM OA, VEGF-A_{165}b did not have an effect. **(C)** Neurite outgrowth was plotted as percentage of DMSO control with and without VEGF-A_{165} treatment. Points=mean, error bars=SEM. *$p<0.05$ compared with PBS, **$p<0.01$ compared with PBS, ***$p<0.001$ compared with PBS, $^{###}p<0.001$ compared with VEGF-A_{165}b. Two way ANOVA with Holm Sidak *post hoc* tests. *N*=3 with six images analysed per repeat.

TABLE 1 Summary table for the effect size and IC_{50} of VEGF-A isoforms on OA-induced neurite "dieback" in SHSY5Y cells.

Co-treatment	PBS(vehicle)	VEGF-A_{165}a	VEGF-A_{165}b
Bottom	Constrained> = 0		
Top	24.18	33.36	24.83
LogIC50	0.479	0.534	0.710
IC50	3.011	3.423	5.133

Values based on *N* = 18 images per condition and quantification of sum neurite outgrowth normalised to the number of cells in field of view.

that VEGF-A_{165}b treatment exerts a stronger protective effect on outgrowth as higher concentration of OA is required to produce the same level of neurite "dieback."

3.4. SRPK1 inhibition can change splicing of VEGF-A in SHSY5Y cells

Sphinx31 is a SRPK1 inhibitor that has been shown to switch splicing from VEGF-A_{165}a to VEGF-A_{165}b in epithelial cells, as well as dorsal root ganglionic cells. Consequentially, Sphinx31 is a

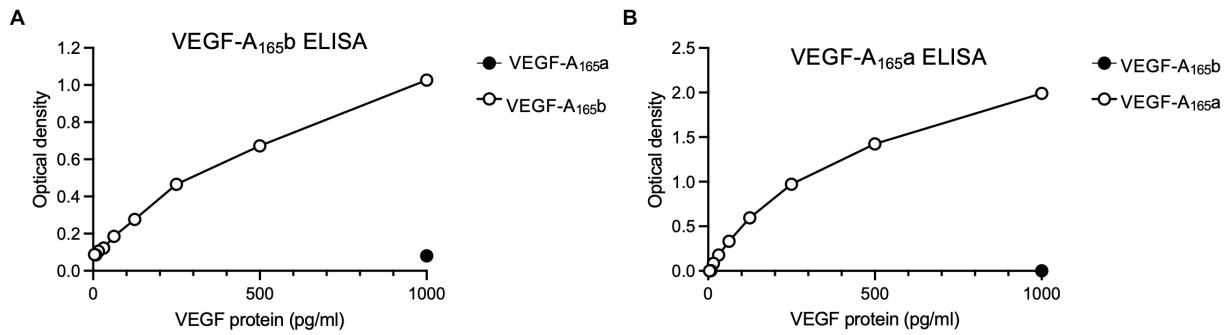

FIGURE 6
Standard curves for the **(A)** VEGF-A_{165}b ELISA and **(B)** VEGF-A_{165}a ELISA, which show detection window for protein expression. Points on each graph are average of two independent ELISA plates, run for SHSY5Y cell lysates and media samples.

powerful investigatory tool for alternative splicing of VEGF-A and other genes regulated by SRPK1. However, Sphinx31 has not been previously used on SHSY5Y cells. Since recombinant VEGF-A_{165}b was shown to have neuroprotective effects in SHSY5Y cells, we aimed to determine whether use of Sphinx31 could increase endogenous expression of VEGF-A_{165}b, and potentially replicate the same physiological results. To quantify relative expression of VEGF-A isoforms, we used a highly sensitive measure of expression, ELISA, to detect relative expression of VEGF-A_{165}a and VEGF-A_{165}b isoforms in SHSY5Y cells. Optimisation of this ELISA is described in the methods, and the standard curves used for relative protein quantification are shown in Figure 6 (minus "blank" i.e., OD measured from 1% BSA only). All values were then normalised to vehicle control group VEGF-A isoform expression.

Expression of both isoforms was detectable in both cell lysate and media collected from SHSY5Y samples. In the cell lysate, VEGF-A_{165}a expression did not change with Sphinx31 treatment (Figure 7A) but VEGF-A_{165}b significantly increased 82.6 ± 7.7% above vehicle control with 1 μM Sphinx31 (Figure 7B, one-way ANOVA, $p < 0.001$). The ratio of VEGF-A_{165}a:VEGF-A_{165}b in cell lysate was calculated to show a significant decrease with both 1 and 10 μM Sphinx31 treatment (shown in Figure 7C, $p < 0.001$ and $p < 0.05$, respectively). However, this effect was not concentration-dependent, suggesting that the lowest concentration 1 μM Sphinx31 was sufficient to induce a shift in VEGF-A splicing towards the VEGF-A_{165}b isoform, and this was the maximal effect observable in SHSY5Y cells through SRPK1 inhibition.

In cell media, VEGF-A_{165}a expression significantly reduced with 10 μM Sphinx31 treatment to 63.5% ± 1.1% of vehicle control, as shown in Figure 7D ($p < 0.0001$, one-way ANOVA). In contrast, VEGF-A_{165}b expression showed a general increase, albeit variable (Figure 7E). At 3 and 10 μM Sphinx31, VEGF-A_{165}b expression was measured to be 97.3 ± 12.2% and 66.6 ± 26.1% higher than vehicle control, respectively ($p < 0.05$ at 3 μM treatment, one-way ANOVA). This caused a significant decrease in the ratio of VEGF-A_{165}a:VEGF-A_{165}b in cell media at both 3 and 10 μM Sphinx31 treatment (Figure 7F). As a measure of secreted protein, this confirms that altered splicing of VEGF-A in Sphinx31-treated SHSY5Y cells can be quantified in both intracellular and extracellular protein.

3.5. SRPK1 inhibition is neuroprotective against tau hyperphosphorylation

Based on the findings that VEGF-A_{165}b can increase outgrowth of SHSY5Y cells and Sphinx31 can shift splicing from VEGF-A_{165}a towards VEGF-A_{165}b, we determined whether 3 μM Sphinx31 treatment would have the same effects on neurite outgrowth as recombinant VEGF-A_{165}b. Using the OA neurotoxicity model (with DMSO vehicle control, representative images shown in Figure 8A), Sphinx31 treatment protected against OA-induced decline in SHSY5Y cell outgrowth. As shown in Figure 8B, OA significantly reduces outgrowth in a concentration-dependent manner, while Sphinx31 ameliorates OA-induced neurite "dieback." At 1 nM OA, Sphinx31-treated cells showed increased neurite outgrowth from an average of 15 ± 1 to 28 ± 1 μm (two-way ANOVA, $p < 0.01$). Similarly, at 3 nM OA, Sphinx31 treatment increased outgrowth from an average of 9 ± 1 to 17 ± 1 μm (two-way ANOVA, $p < 0.0001$). At 10 nM OA, Sphinx31 treatment was no longer neuroprotective. In fact, outgrowth was effectively ablated with this treatment combination, as very few cells were observed compared to the control group (Figure 8A). Similar results were seen in previous iterations of this assay with PBS vehicle control, which could imply that DMSO alone may affect outgrowth.

3.5.1. SRPK1 inhibition is neuroprotective through a VEGF-A_{165}b mediated mechanism

To determine whether the neuroprotective effect of Sphinx31 is dependent on alternative splicing of VEGF-A, the outgrowth assay was repeated with a VEGF-A_{165}b neutralising antibody co-treatment (Figure 8B). Compared to Sphinx31 alone, anti-VEGF-A_{165}b-treated SHSY5Y cells showed significantly reduced outgrowth (Figure 8B), indicating that amelioration of outgrowth with Sphinx31 does in fact occur, at least partially, through increased VEGF-A_{165}b expression. In the presence of 1 and 3 nM OA respectively, when co-treated with both Sphinx31 and

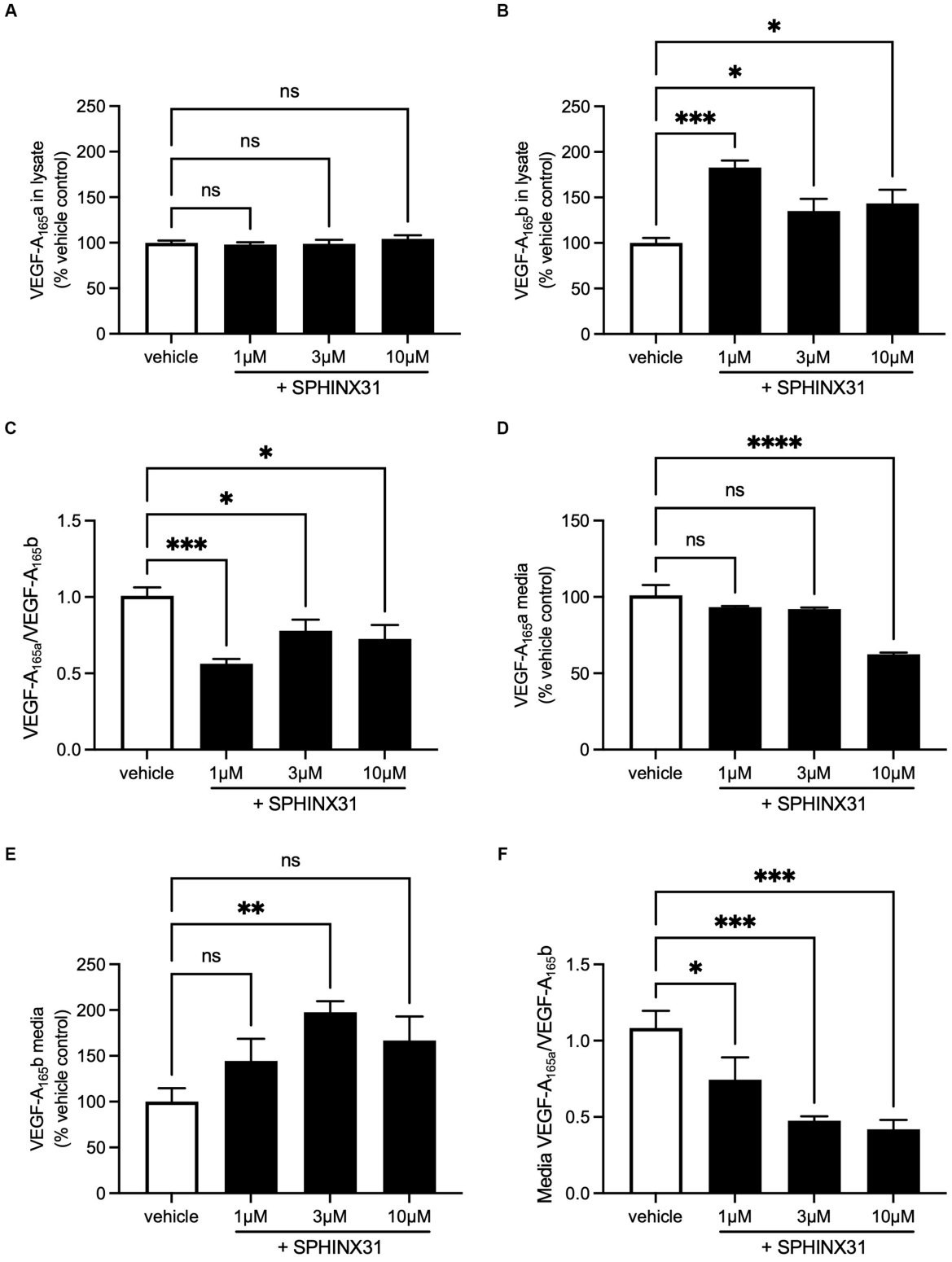

FIGURE 7
Sphinx31 treatment significantly reduces VEGF-A_{165}a:VEGF-A_{165}b ratio expression in SHSY5Y cells. **(A)** Sphinx31 does not produce measurable change in VEGF-A_{165}a expression in cell lysate. **(B)** Cell lysate shows a significant increase in VEGF-A_{165}b Sphinx31 (p<0.001). **(C)** The ratio of VEGF-A_{165}a:VEGF-A_{165}b is significantly reduced in cell lysate with Sphinx31 treatment, but this does not occur in a concentration-dependent manner (p<0.001 one-way ANOVA). **(D)** VEGF-A_{165}a in cell media remains stable with 1–3μM Sphinx31 but is significantly reduced with 10μM treatment (p<0.0001, one-way ANOVA). **(E)** There was an increase in VEGF-A_{165}b in the media with Sphinx31 treatment. Measured increase with 3μM is statistically significant (p<0.05, one-way ANOVA). **(F)** The ratio of VEGF-A_{165}a:VEGF-A_{165}b is dose dependently reduced in media after treatment with Sphinx31 (p<0.001 and p<0.05, one-way ANOVA). N=3 biological replicates and N=2 technical replicates.

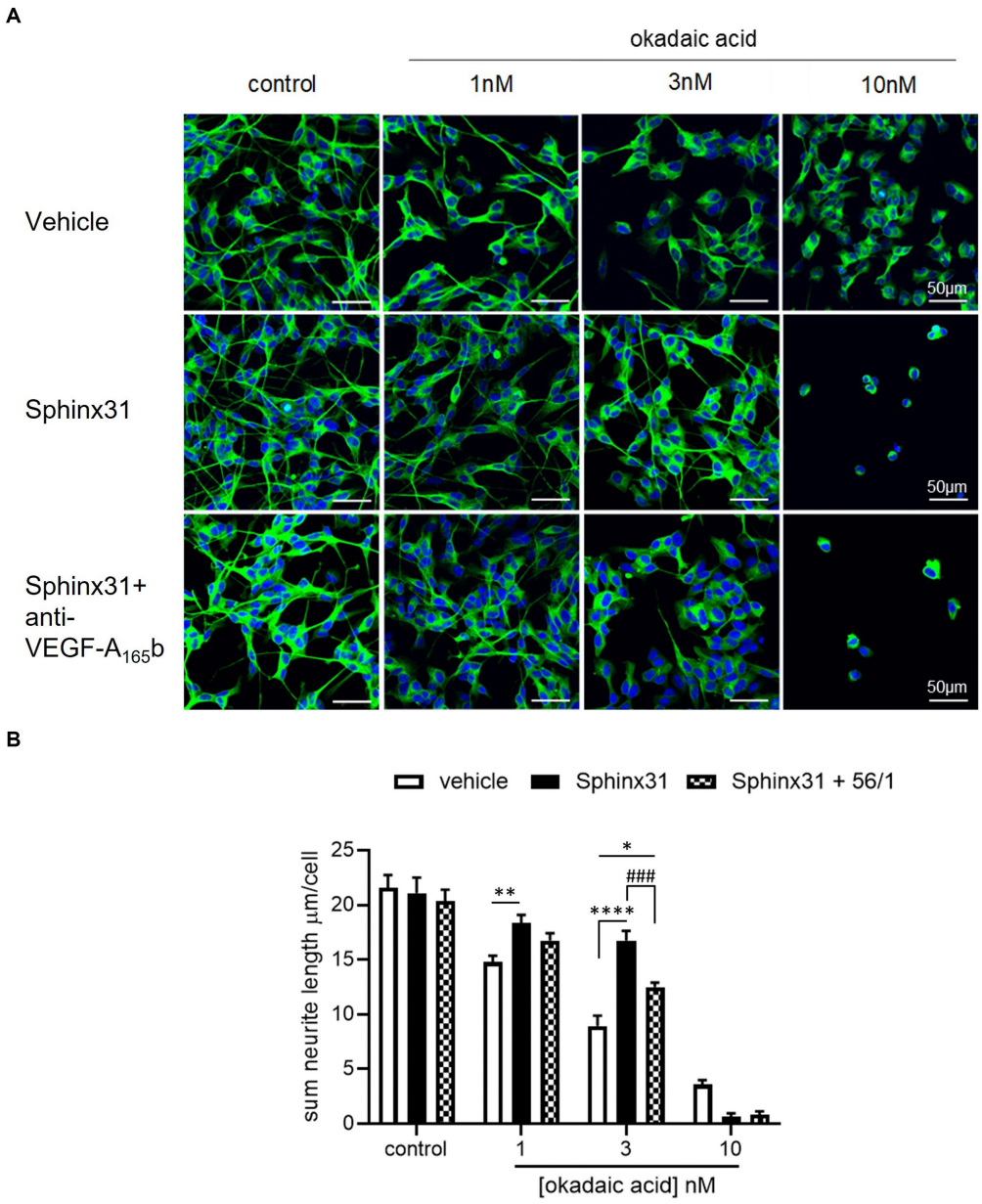

FIGURE 8
Sphinx31 significantly ameliorates OA-induced decline in neurite outgrowth from SHSY5Y cells. **(A)** neuron-specific marker βIII tubulin identified neurites in green. Cell nuclei stained with Hoechst shown in blue. Neurite outgrowth was calculated by tracing neurites on Image J and dividing the sum length per image by the number of cells. The top row of images shows OA vehicle alone, the middle row shows co-treatment with Sphinx31, the bottom row treatment with Sphinx31 and anti-VEGF-A_{165}b. **(B)** Sphinx31 co-treatment significantly ameliorates decline in neurite outgrowth induced by 1 and 3nM OA, which was inhibited by treatment with anti-VEGF-A_{165}b (two-way ANOVA, $p<0.01$ and $p<0.0001$, respectively). $N=2$ with six images analysed per repeat. Error bars=SEM.

anti-VEGF-A_{165}b, there was a significant reduction in neurite outgrowth compared to Sphinx31 alone, at an average sum length of 13 ± 0.5 µm (two-way ANOVA, $p < 0.001$, Figure 8B). However, this remained significantly higher than the control group at 3 nM OA (two-way ANOVA, $p < 0.05$). It is possible that (a) anti-VEGF-A_{165}b treatment did not completely ablate VEGF-A_{165}b at concentration 1 ng/mL, or (b) Sphinx31 is neuroprotective through other mechanisms in addition to VEGF-A alternative splicing.

3.5.2. OA and Sphinx31 treatments do not significantly alter the 4R:3R tau ratio in SHSY5Y cells

Okadaic acid was used here to model AD-related neurotoxicity, since OA is known to induce hyperphosphorylation of tau (Martin et al., 2011). However, the relative expression of 4R and 3R tau isoforms is also important to AD pathology (Espindola et al., 2018). Since SRPK1 is a splicing kinase, and Sphinx31 is a selective and potent SRPK1 inhibitor, we determined whether Sphinx31 and OA co-treatment

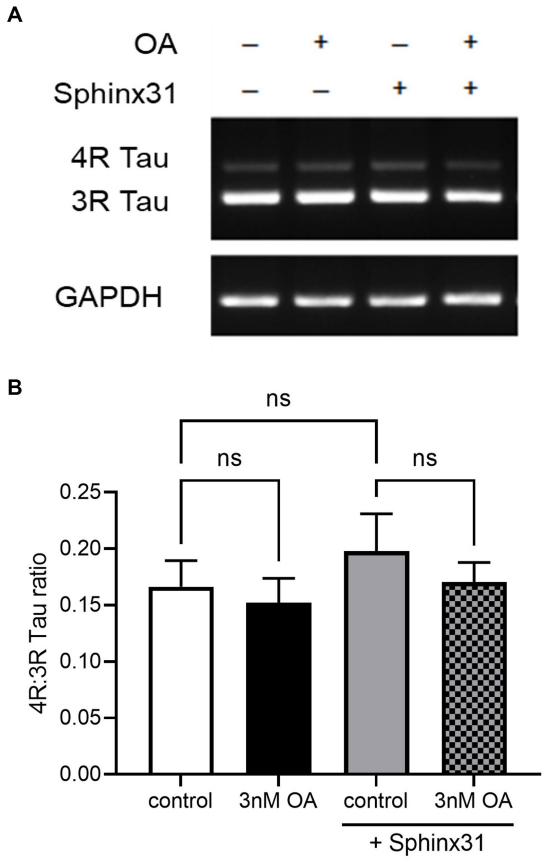

FIGURE 9
OA and Sphinx31 treatments do not significantly alter the 4R:3R tau ratio in SHSY5Y cells. **(A)** SHSY5Y cells were treated with 3nM OA and/or 3μM Sphinx31 for 24h. *MAPT* PCR was carried out using primers spanning exon 10 (forward primer in exon 9, reverse primer in exon 11) to quantify relative expression of 4R and 3R tau isoforms. Images show tau isoform expression and housekeeping gene *GAPDH* matched to each sample. **(B)** Sphinx31 treatment does not significantly alter 4R:3R tau ratio (one-way ANOVA, $p>0.05$). $N=4$, error bars show SEM.

caused a shift in the 4R:3R tau ratio. Note that although SHSY5Y cells preferentially express 3R tau, they do endogenously express both 4R and 3R tau isoforms. Sphinx31 treatment showed slightly increased 4R:3R tau ratio, quantified to be 32 ± 7% higher than control group (Figure 9). However, this change was not statistically significant, and 3 nM OA treatment did not induce a significant shift in the 4R:3R tau ratio either (one-way ANOVA, $p>0.05$). This indicates that the observed physiological effect of Sphinx31 on outgrowth is not dependent on alternative splicing of the *MAPT* gene. The vehicle for both OA and Sphinx31 is DMSO, thus all values were normalised to 0.02% DMSO treated control group.

4. Discussion

There are numerous *in vitro* models for AD that incorporate different aspects of its pathology. To investigate the neuroprotective properties of VEGF-A isoforms, it was necessary to develop a robust neurotoxicity assay that consistently presented concentration-dependent cell death within a reasonable range and that could be rescued by neuroprotective agents.

4.1. VEGF-A_{165} isoforms increase viability of SHSY5Y cells in oxidative stress *in vitro* model

Hydrogen peroxide was used to create an oxidative stress model in SHSY5Y cells. In both SHSY5Y and N2a cell lines, NGF treatment evoked a significant increase in cell viability. When treated with either VEGF-A_{165}a or VEGF-A_{165}b, SHSY5Y cells demonstrated a similar increase in metabolic activity comparable to that without H_2O_2. This is in alignment with other studies, which have demonstrated VEGF-A dependent neuroprotection (Beazley-Long et al., 2013) and supports the hypothesis that VEGF-A treatment can increase neuronal viability in the presence of oxidative stress. There was not an observable difference in the effect of alternative splicing isoforms which suggests that despite having opposing effects on angiogenesis (Nowak et al., 2010) both splicing families maintain neuroprotective effects in SHSY5Y cells.

However, VEGF-A induced increase in cell viability was not reproduced in N2a cells. This could be attributed, at least in part, to the smaller cell viability window where relatively low concentrations of hydrogen peroxide (e.g., 50 μM) reduced cell viability to less than half of control. There is limited published data surrounding VEGF-A function in N2a cells, but it has been reported that inhibition of VEGF-A with a neutralising antibody increases N2a cellular viability under hypoxic conditions (Saraswat et al., 2015). This finding was related to maintaining normal levels of VEGF-A since it is upregulated by hypoxia via hypoxia-inducible factor-1 (HIF-1). Since HIF-1 is also known to be upregulated by reactive oxygen species, including H_2O_2 (Bonello et al., 2007) it could be postulated that VEGF-A was already upregulated and no longer exerting cytoprotective effects, explaining why we could not measure a significant change in N2a viability. The VEGF-A_{165}b isoform did not significantly affect N2a viability either, despite evidence that VEGF-A_{165}b can negatively regulate VEGFR2 expression (Ballmer-Hofer et al., 2011) which would arguably counteract HIF-1 induced VEGF-A activity. However, VEGF-A_{165}b remains a partial agonist of VEGFR2 (Kawamura et al., 2008) and is dependent on VEGFR2 to elicit neuroprotection (Beazley-Long et al., 2013). Therefore, it is not appropriate to compare VEGF-A_{165}b mediated neuroprotection with that related to VEGF-A neutralisation. It is also important to note that Saraswat et al. did not measure VEGFR2 expression or activation, and it is likely that blocking VEGF-A activity would have caused upregulation of VEGFR2 through the clathrin-mediated pathway (Bruns et al., 2010). VEGFR2 trafficking could also explain the lack of response seen in N2a cells if HIF-1 induced VEGF-A expression resulted in VEGFR2 internalisation. For future work, and more comprehensive understanding of neuronal VEGF-A signalling, treatment with recombinant VEGF-A isoforms could be repeated in the presence of an VEGFR2 inhibitor.

4.2. Both types of VEGF-A_{165} isoforms increase viability of SHSY5Y cells in amyloid *in vitro* model

The amyloid *in vitro* model was able to induce loss of viability in N2a cells and a significant reduction in SHSY5Y cells. This observation was consistent with previously published work optimising treatment methods of amyloid in various states (Stine et al., 2011). In its

unaggregated state, 1 μM amyloid was found to decrease N2a cell survival. In other studies carried out in SHSY5Y cells, amyloid treatment between 1 and 10 μM was successfully used to induce neurotoxicity (Stine et al., 2011; Hettiarachchi et al., 2014; Zheng et al., 2014). As seen in Figure 3, both VEGF-A_{165}a and VEGF-A_{165}b completely rescued the amyloid-induced decrease in SHSY5Y cell viability. This complements results from the oxidative stress *in vitro* model and confirms that both splicing isoforms are able to rescue neurotoxic effects associated with the accumulation of amyloid.

4.3. VEGF-A_{165}a increases neurite outgrowth of SHSY5Y cells in tau hyperphosphorylation *in vitro* model

In AD and many other tauopathies, NFTs result from the hyperphosphorylation of tau and its aggregation within neurones (Bancher et al., 1989). Regulation of tau function is dependent on glycogen synthase kinase 3β (GSK-3β) and protein phosphatase 2A (PP2A) enzymes which play a role in tau phosphorylation and dephosphorylation, respectively, (Gong and Iqbal, 2008). In fact, PP2A activity is decreased by ~30% in AD brain (Gong et al., 1995), highlighting its importance in the regulation of normal tau function. Okadaic acid (OA) has been used a potent inhibitor of PP2A to induce tau hyperphosphorylation *in vitro* (Martin et al., 2011). In the development of this neurotoxicity model (as seen in Figure 4), we showed that OA decreases neurite outgrowth of SHSY5Y cells in a concentration-dependent manner. This neurotoxic effect of OA is in alignment with observations from similar studies using OA in SHSY5Y cells (Metin-Armagan et al., 2018; Boban et al., 2019).

Okadaic acid treatment has also been shown to upregulate VEGF-A expression (Wakiya and Shibuya, 1999), which is closely related to increased activity of HIF-1 activated by the mTOR pathway (Kim et al., 2009). While PP2A inhibits ribosomal protein S6 kinase (S6K) activity, VEGFR2 promotes mTOR signalling and PKC activation, which positively regulates S6K. Therefore, OA inhibition of PP2A significantly increases VEGF-A mediated PKC activation and S6K activity (Edelstein et al., 2011) which is yet further augmented by treatment with recombinant VEGF-A. As well as controlling protein synthesis, S6K activity is known to signal cell survival (Harada et al., 2001) which may account (or at least contribute towards) the cytoprotective properties of VEGF-A. In this study, VEGF-A_{165}a treatment amplified neurite outgrowth in the absence and presence of OA; this can be observed in Figure 6, which shows an upward shift in SHSY5Y neurite outgrowth in the presence of 0–3 nM OA. This could be mediated by an upregulation of S6K activity, suggesting that VEGF-A could compensate for loss of neuronal function related to tau hyperphosphorylation. When coupled with previous experiments that showed recovery of amyloid-induced decrease in cell viability, it can be concluded that VEGF-A is protective against both forms of AD-related neurotoxicity.

4.4. VEGF-A_{165}b recovers the decrease in neurite outgrowth of SHSY5Y cells in tau hyper-phosphorylation *in vitro* model

As opposed to VEGF-A_{165}a, a full agonist of endothelial VEGFR2 that stabilises its interaction with NP-1, VEGF-A_{165}b is a partial agonist of endothelial VEGFR2 that is unable to bind NP-1 and promotes internalisation and degradation of VEGFR2 (Ballmer-Hofer et al., 2011). Consequentially, VEGF-A_{165}a binding leads to PKC activation while VEGF-A_{165}b binding does not (Kisko et al., 2011; Hulse et al., 2014). Since PKC is a negative regulator of Akt, its inhibition has been shown to increase Akt phosphorylation (Edelstein et al., 2011). Akt is known to inhibit GSK-3β activity (Hermida et al., 2017), which in turn phosphorylates tau (Gong and Iqbal, 2008). If VEGF-A_{165}b is able to downregulate neuronal VEGFR2 in a similar way to endothelial VEGFR2, it could be postulated that resulting Akt inhibition of GSK-3β protects against tau hyperphosphorylation and could therefore have knock-on effects on tau function.

In this study, VEGF-A_{165}b co-treatment alone did not increase neurite outgrowth of SHSY5Y cells. However, VEGF-A_{165}b protected against the decrease in neurite outgrowth seen with 1 and 3 nM OA, as observed by the rightward curve shift in Figure 5 where there is no measured decrease in neurite outgrowth compared to control. This indicates that VEGF-A_{165}b is not ubiquitously increasing neurite outgrowth but acting directly against the effect of OA. This could potentially occur via the PI3/Akt pathway: if VEGF-A_{165}b causes downregulation of VEGFR2 and attenuates PKC activation, it may lead to increased Akt phosphorylation, greater inhibition of GSK-3β activity, and thus reduced phosphorylation of tau. If sufficient to counter-act OA inhibition of PP2A, this could prevent the hyperphosphorylation of tau and thus protect against downstream effects, including decrease in neurite outgrowth.

4.5. SRPK1 inhibitor Sphinx31 significantly decreases VEGF-A_{165}a:VEGF-A_{165}b ratio in SHSY5Y cells

SRPK1 is related to alternative splicing of VEGF-A through phosphorylation of SRSF1 (Harper and Bates, 2008). SRPK1 activity drives nuclear localisation of SRSF1 and promotes selection of the proximal splice site in exon 8 in epithelial cells, producing-A_{165}a (Nowak et al., 2008). SRPK1 inhibition reduces phosphorylation of SRSF1 and consequentially increases selection of the distal splice site in exon 8, producing VEGF-A_{165}b (Nowak et al., 2010). This has been established through use of SRPK1 inhibiting compounds SRPN340 and Sphinx31 in a variety of tissues, including the kidney (Amin et al., 2011), retinal epithelium (Gammons et al., 2013; Batson et al., 2017), peripheral neurones (Hulse et al., 2014), prostate cancer (Mavrou and Oltean, 2016), and acute myeloid leukaemia (Tzelepis et al., 2018). Consequently, alternative VEGF-A splicing has been related to a number of pathological conditions, including Denys Drash Syndrome, diabetic retinopathy, age-related wet macular degeneration (AMD), neuropathic pain, and cancer. However, Sphinx31 (or SRPK1 inhibition) had not been previously investigated in SHSY5Y cells, used here as a neuronal model. As shown in Figure 7, SRPK1 inhibition does modulate VEGF-A exon 8 splicing in SHSY5Y cells, making them a viable model to investigate the neuroprotective role of VEGF-A isoforms in AD-related neurotoxicity. Consistent with the effect observed in other tissues, both intracellular and extracellular VEGF-A showed a proportional shift towards the VEGF-A_{165}b isoform and significant decrease in VEGF-A_{165}a:VEGF-A_{165}b ratio. Of interest it also

changed the secretion level of the two isoforms, a phenomenon previously shown in neuroblastoma cells (Peiris-Pages et al., 2010). It is possible that SRPK1 inhibition could also change the secretion by changing the RNA sub-compartment of the different RNAs (Hamdollah Zadeh et al., 2015).

4.6. SRPK1 inhibition recovers OA-induced decrease in neurite outgrowth and recovery is dependent on endogenous VEGF-A_{165}b

Similar to observed effects of recombinant VEGF-A_{165}b, Sphinx31 treatment was shown to protect against OA-induced decrease in neurite outgrowth. In the presence of 1 and 3 nM OA, Sphinx31 co-treatment significantly increased outgrowth to a level comparable to vehicle control (see Figure 8). This is a novel finding which suggests SRPK1 inhibition is neuroprotective in the OA model for tau hyperphosphorylation. When SHSY5Y cells were co-treated with Sphinx31 and a VEGF-A_{165}b-neutralising antibody (Figure 8), amelioration of neurite outgrowth was significantly reduced. As a result, it can be concluded that the neuroprotective effect of Sphinx31 is dependent on VEGF-A_{165}b expression, which increases relative to VEGF-A_{165}a with SRPK1 inhibition. However, anti-VEGF-A_{165}b-treated SHSY5Y cells still showed significantly higher outgrowth than OA control, demonstrating that the Sphinx31 effect is not completely ablated. This suggests that SRPK1 inhibition could be neuroprotective through other targets, not just via VEGF-A alternative splicing.

Recombinant VEGF-A_{165}b has been reported as a neuroprotective agent in response to numerous insults, including glutamatergic excitotoxicity in hippocampal neurones, chemotherapy-induced cytotoxicity of dorsal root ganglia, and ischaemia-reperfusion injury in retina (Beazley-Long et al., 2013). Therefore, the main findings here are consistent with previous work and confirm that Sphinx31 can be used as a tool to switch VEGF-A splicing and replicate the neuroprotective effect of VEGF-A_{165}b in the OA model for tau hyperphosphorylation. Beazley-Long et al. (2013) reported that the neuroprotective action of VEGF-A_{165}b in hippocampal neurones was mediated through VEGFR2, as it was blocked by VEGFR2 inhibitors but maintained with selective R1 inhibition. It was also found that hippocampal neuroprotection was unaffected by inhibition of PI3K or p38 MAPK, supporting the previously discussed hypothesis that VEGF-A_{165}b acts as a partial agonist at VEGFR2 and does not activate the mTOR pathway (Ballmer-Hofer et al., 2011). Similarly, Sphinx31-mediated VEGF-A_{165}b expression seems to act against canonical VEGF-A_{165}a signalling, preventing activation of PKC and phosphorylation of PI3K (Harper and Bates, 2008). Therefore, Sphinx31 is likely to exert neuroprotection through another pathway. Beazley-Long et al. (2013) suggest involvement of MEK1/2 pathway because VEGF-A_{165}b was shown to induce Erk1/2 phosphorylation, which has been independently shown to ameliorate neuronal damage (Bhowmick et al., 2019). However, activation of Erk1/2 is thought to be altered in AD pathology and has been related to hyperphosphorylation of tau and increased NFT burden (Pei et al., 2002; Veeranna et al., 2004).

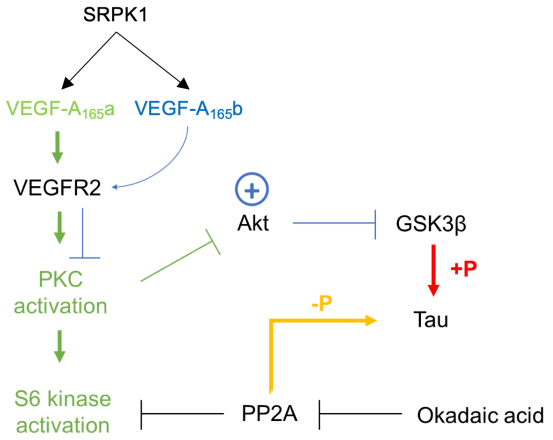

FIGURE 10
Schematic summarising proposed action of VEGF-A_{165}a and VEGF-A_{165}b via VEGFR2 binding and full or partial agonism, respectively. Green path represents VEGF-A_{165}a activation, blue path represents VEGF-A_{165}b activation.

Considering OA-induced neurotoxicity is based on tau phosphorylation, it would be contradictory to suggest that VEGF-A_{165}b-mediated neuroprotection occurred through a mechanism that is known to further phosphorylate tau. It is possible therefore that VEGF-A_{165}b (and by extension Sphinx31) dependent neuroprotection occurs through aforementioned inhibition of GSK-3β activity (Figure 10). As this hypothesis is mostly based on evidence from endothelial cells, it would be necessary to empirically test VEGF-A_{165}b binding to neuronal VEGFR2 and activation of downstream targets, most notable GSK-3β, in SHSY5Y cells to definitively conclude how neuronal VEGF-A_{165}b functions.

There are some limitations to this study. We have only examined one cell line, and additional work on Sphinx31 could focus on investigating its effect on primary neurons such as those used by Beazley-Long et al. (2013), and it is not known whether Sphinx31 is neuroprotective in these contexts. The most closely related data published on the effect of Sphinx31 in nervous tissue identified its use for analgesia: Treatment of primary afferents and resultant shift towards VEGF-A_{165}b expression was found to lower VEGF-A_{165}a mediated sensitisation of mechanical nociceptors to stimulation (Hulse et al., 2014). Together with data presented here, this identifies SRPK1 inhibition as an interesting therapeutic target in the CNS as well as the PNS, with potential applications in neuroprotection. An additional limitation is that we have measured the protein isoform switch by ELISA using isoform selective antibodies, but it is possible that these ELISAs also detect VEGF-A_{121}b or VEGF-A_{189}b, and VEGF-A_{121}a or VEGF-A_{189}a, respectively, so immunoblotting would be useful. However, the VEGF-A_{xxx}a antibody (a Fab fragment) is not optimised for immunoblotting and would need to be modified to do so. With regards to AD, it would be extremely useful to extend the findings on VEGF isoform neuroprotection on OA induced effects to other neuronal types, perhaps using neurons differentiated from iPSC cells. It would also be interesting to explore the effect of Sphinx31 on other aspects of its pathology, perhaps using the AD transgenic mouse model, and

determine whether *in vitro* results translate *in vivo*. Finally, to show the specificity of the proposed mechanism it would be useful to reinforce the proposed mechanism, for example, by evaluation of the effect of siRNA- or CRISPR-mediated inactivation of SRPK1 and VEGF.

Data availability statement

The raw data supporting the conclusions of this article will be made available by the authors, without undue reservation.

Author contributions

LD, DB, RA, and KM contributed to conception and design of the study. TH and JM synthesised the Sphinx31. RA undertook the experiments and wrote the first draft of the manuscript. RA, LD, and DB undertook analysis. DB and LD wrote the sections of the manuscript. All authors contributed to the article and approved the submitted version.

Funding

This work was funded by the University of Nottingham BBSRC Doctoral Training Programme (Grant BB/M008770/1).

Acknowledgments

RA would like to acknowledge all members of the Tumour and Vascular Biology Laboratories at the University of Nottingham for their support and encouragement.

Conflict of interest

LD, DB, and JM are founders and stock-holders in Exonate Ltd., a company that is developing SRPK1 inhibitors for clinical use. LD and JM are founders and stockholders in Emenda Therapeutics, a company that is developing splicing factor kinase inhibitors for therapeutic use.

The remaining authors declare that the research was conducted in the absence of any commercial or financial relationships that could be construed as a potential conflict of interest.

Publisher's note

References

Amin, E. M., Oltean, S., Hua, J., Gammons, M. V. R., Hamdollah-Zadeh, M., Welsh, G. I., et al. (2011). WT1 mutants reveal SRPK1 to be a downstream angiogenesis target by altering VEGF splicing. *Cancer Cell* 20, 768–780. doi: 10.1016/j.ccr.2011.10.016

Ballmer-Hofer, K., Andersson, A. E., Ratcliffe, L. E., and Berger, P. (2011). Neuropilin-1 promotes VEGFR-2 trafficking through Rab11 vesicles thereby specifying signal output. *Blood* 118, 816–826. doi: 10.1182/blood-2011-01-328773

Bancher, C., Brunner, C., Lassmann, H., Budka, H., Jellinger, K., Wiche, G., et al. (1989). Accumulation of abnormally phosphorylated tau precedes the formation of neurofibrillary tangles in Alzheimer's disease. *Brain Res.* 477, 90–99.

Batson, J., Toop, H. D., Redondo, C., Babaei-Jadidi, R., Chaikuad, A., Wearmouth, S. F., et al. (2017). Development of potent, selective SRPK1 inhibitors as potential topical therapeutics for Neovascular eye disease. *ACS Chem. Biol.* 12, 825–832. doi: 10.1021/acschembio.6b01048

Beazley-Long, N., Hua, J., Jehle, T., Hulse, R. P., Dersch, R., Lehrling, C., et al. (2013). VEGF-A165b is an endogenous Neuroprotective splice isoform of vascular endothelial growth factor a in vivo and in vitro. *Am. J. Pathol.* 183, 918–929. doi: 10.1016/j.ajpath.2013.05.031

Bhowmick, S., D'Mello, V., and Abdul-Muneer, P. M. (2019). Synergistic inhibition of ERK1/2 and JNK, not p38, phosphorylation ameliorates neuronal damages after traumatic Brain injury. *Mol. Neurobiol.* 56, 1124–1136. doi: 10.1007/s12035-018-1132-7

Boban, M., Babic Leko, M., Miskic, T., Hof, P. R., and Simic, G. (2019). Human neuroblastoma SH-SY5Y cells treated with okadaic acid express phosphorylated high molecular weight tau-immunoreactive protein species. *J. Neurosci. Methods* 319, 60–68. doi: 10.1016/j.jneumeth.2018.09.030

Bogetti, M. E., Pozo Devoto, V. M., Rapacioli, M., Flores, V., and Fiszer de Plazas, S. (2018). NGF, TrkA-P and neuroprotection after a hypoxic event in the developing central nervous system. *Int. J. Dev. Neurosci.* 71, 111–121. doi: 10.1016/j.ijdevneu.2018.08.007

Bonello, S., Zahringer, C., BelAiba, R. S., Djordjevic, T., Hess, J., Michiels, C., et al. (2007). Reactive oxygen species activate the HIF-1alpha promoter via a functional NFkappaB site. *Arterioscler. Thromb. Vasc. Biol.* 27, 755–761. doi: 10.1161/01.ATV.0000258979.92828.bc

Bruns, A. F., Herbert, S. P., Odell, A. F., Jopling, H. M., Hooper, N. M., Zachary, I. C., et al. (2010). Ligand-stimulated VEGFR2 signaling is regulated by co-ordinated trafficking and proteolysis. *Traffic* 11, 161–174. doi: 10.1111/j.1600-0854.2009.01001.x

Cheignon, C., Tomas, M., Bonnefont-Rousselot, D., Faller, P., Hureau, C., and Collin, F. (2018). Oxidative stress and the amyloid beta peptide in Alzheimer's disease. *Redox Biol.* 14, 450–464. doi: 10.1016/j.redox.2017.10.014

Draberova, E., Lukas, Z., Ivanyi, D., Viklicky, V., and Draber, P. (1998). Expression of class III beta-tubulin in normal and neoplastic human tissues. *Histochem. Cell Biol.* 109, 231–239.

Edelstein, J., Hao, T., Cao, Q., Morales, L., and Rockwell, P. (2011). Crosstalk between VEGFR2 and muscarinic receptors regulates the mTOR pathway in serum starved SK-N-SH human neuroblastoma cells. *Cell. Signal.* 23, 239–248. doi: 10.1016/j.cellsig.2010.09.008

Espindola, S. L., Damianich, A., Alvarez, R. J., Sartor, M., Belforte, J. E., Ferrario, J. E., et al. (2018). Modulation of tau isoforms imbalance precludes tau pathology and cognitive decline in a mouse model of Tauopathy. *Cell Rep.* 23, 709–715. doi: 10.1016/j.celrep.2018.03.079

Gammons, M. V., Fedorov, O., Ivison, D., Du, C., Clark, T., Hopkins, C., et al. (2013). Topical Antiangiogenic SRPK1 inhibitors reduce Choroidal neovascularization in rodent models of exudative AMD. *Invest. Ophthalmol. Vis. Sci.* 54, 6052–6062. doi: 10.1167/iovs.13-12422

Gong, C. X., and Iqbal, K. (2008). Hyperphosphorylation of microtubule-associated protein tau: a promising therapeutic target for Alzheimer disease. *Curr. Med. Chem.* 15, 2321–2328. doi: 10.2174/092986708785909111

Gong, C. X., Shaikh, S., Wang, J. Z., Zaidi, T., Grundke-Iqbal, I., and Iqbal, K. (1995). Phosphatase activity towards abnormally phosphorylated tau: decrease in Alzheimer disease brain. *J. Neurochem.* 65, 732–738.

Greenberg, D. A., and Jin, K. L. (2005). From angiogenesis to neuropathology. *Nature* 438, 954–959. doi: 10.1038/nature04481

Hamdollah Zadeh, M. A., Amin, E. M., Hoareau-Aveilla, C., Domingo, E., Symonds, K. E., Ye, X., et al. (2015). Alternative splicing of TIA-1 in human colon cancer regulates VEGF isoform expression, angiogenesis, tumour growth and bevacizumab resistance. *Mol. Oncol.* 9, 167–178. doi: 10.1016/j.molonc.2014.07.017

Harada, H., Andersen, J. S., Mann, M., Terada, N., and Korsmeyer, S. J. (2001). p70S6 kinase signals cell survival as well as growth, inactivating the pro-apoptotic molecule

BAD. *Proc. Natl. Acad. Sci. U. S. A.* 98, 9666–9670. doi: 10.1073/pnas.171301998

Harari, O., Cruchaga, C., Kauwe, J. S., Ainscough, B. J., Bales, K., Pickering, E. H., et al. (2014). Phosphorylated tau-Abeta42 ratio as a continuous trait for biomarker discovery for early-stage Alzheimer's disease in multiplex immunoassay panels of cerebrospinal fluid. *Biol. Psychiatry* 75, 723–731. doi: 10.1016/j.biopsych.2013.11.032

Harper, S. J., and Bates, D. O. (2008). VEGF-A splicing: the key to anti-angiogenic therapeutics? *Nat. Rev. Cancer* 8, 880–887. doi: 10.1038/nrc2505

Harris, R., Miners, J. S., Allen, S., and Love, S. (2018). VEGFR1 and VEGFR2 in Alzheimer's disease. *J. Alzheimers Dis.* 61, 741–752. doi: 10.3233/JAD-170745

Hermida, M. A., Dinesh Kumar, J., and Leslie, N. R. (2017). GSK3 and its interactions with the PI3K/AKT/mTOR signalling network. *Adv. Biol. Regul.* 65, 5–15. doi: 10.1016/j.jbior.2017.06.003

Hettiarachchi, N. T., Dallas, M. L., Al-Owais, M. M., Griffiths, H. H., Hooper, N. M., Scragg, J. L., et al. (2014). Heme oxygenase-1 protects against Alzheimer's amyloid-beta(1-42)-induced toxicity via carbon monoxide production. *Cell Death Dis.* 5:e1569. doi: 10.1038/cddis.2014.529

Hobson, M. I., Green, C. J., and Terenghi, G. (2000). VEGF enhances intraneural angiogenesis and improves nerve regeneration after axotomy. *J. Anat.* 197, 591–605. doi: 10.1046/j.1469-7580.2000.19740591.x

Hulse, R. P., Beazley-Long, N., Hua, J., Kennedy, H., Prager, J., Bevan, H., et al. (2014). Regulation of alternative VEGF-A mRNA splicing is a therapeutic target for analgesia. *Neurobiol. Dis.* 71, 245–259. doi: 10.1016/j.nbd.2014.08.012

Hulse, R. P., Beazley-Long, N., Ved, N., Bestall, S. M., Riaz, H., Singhal, P., et al. (2015). Vascular endothelial growth factor-A165b prevents diabetic neuropathic pain and sensory neuronal degeneration. *Clin. Sci. (Lond.)* 129, 741–756. doi: 10.1042/CS20150124

Iqbal, K., Liu, F., Gong, C. X., and Grundke-Iqbal, I. (2010). Tau in Alzheimer disease and related tauopathies. *Curr. Alzheimer Res.* 7, 656–664. doi: 10.2174/156720510793611592

Kawamura, H., Li, X., Harper, S. J., Bates, D. O., and Claesson-Welsh, L. (2008). Vascular endothelial growth factor (VEGF)-A165b is a weak in vitro agonist for VEGF receptor-2 due to lack of coreceptor binding and deficient regulation of kinase activity. *Cancer Res.* 68, 4683–4692. doi: 10.1158/0008-5472.CAN-07-6577

Kim, Y. S., Ahn, K. H., Kim, S. Y., and Jeong, J. W. (2009). Okadaic acid promotes angiogenesis via activation of hypoxia-inducible factor-1. *Cancer Lett.* 276, 102–108. doi: 10.1016/j.canlet.2008.10.034

Kisko, K., Brozzo, M. S., Missimer, J., Schleier, T., Menzel, A., Leppanen, V. M., et al. (2011). Structural analysis of vascular endothelial growth factor receptor-2/ligand complexes by small-angle X-ray solution scattering. *FASEB J.* 25, 2980–2986. doi: 10.1096/fj.11-185397

Lindwall, G., and Cole, R. D. (1984). Phosphorylation affects the ability of tau protein to promote microtubule assembly. *J. Biol. Chem.* 259, 5301–5305. doi: 10.1016/S0021-9258(17)42989-9

Martin, L., Page, G., and Terro, F. (2011). Tau phosphorylation and neuronal apoptosis induced by the blockade of PP2A preferentially involve GSK3beta. *Neurochem. Int.* 59, 235–250. doi: 10.1016/j.neuint.2011.05.010

Mavrou, A., and Oltean, S. (2016). SRPK1 inhibition in prostate cancer: a novel anti-angiogenic treatment through modulation of VEGF alternative splicing. *Pharmacol. Res.* 107, 276–281. doi: 10.1016/j.phrs.2016.03.013

Metin-Armagan, D., Gezen-Ak, D., Dursun, E., Atasoy, I. L., Karabay, A., Yilmazer, S., et al. (2018). Okadaic acid-induced tau hyperphosphorylation and the downregulation of Pin1 expression in primary cortical neurons. *J. Chem. Neuroanat.* 92, 41–47. doi: 10.1016/j.jchemneu.2018.05.006

Nowak, D. G., Amin, E. M., Rennel, E. S., Hoareau-Aveilla, C., Gammons, M., Damodoran, G., et al. (2010). Regulation of vascular endothelial growth factor (VEGF) splicing from pro-angiogenic to anti-angiogenic isoforms a NOVEL THERAPEUTIC STRATEGY FOR ANGIOGENESIS. *J. Biol. Chem.* 285, 5532–5540. doi: 10.1074/jbc.M109.074930

Nowak, D. G., Woolard, J., Amin, E. M., Konopatskaya, O., Saleem, M. A., Churchill, A. J., et al. (2008). Expression of pro- and anti-angiogenic isoforms of VEGF is differentially regulated by splicing and growth factors. *J. Cell Sci.* 121, 3487–3495. doi: 10.1242/jcs.016410

Paris, D., Townsend, K., Quadros, A., Humphrey, J., Sun, J., Brem, S., et al. (2004). Inhibition of angiogenesis by Abeta peptides. *Angiogenesis* 7, 75–85. doi: 10.1023/B:AGEN.0000037335.17717.bf

Patel, N. S., Mathura, V. S., Bachmeier, C., Beaulieu-Abdelahad, D., Laporte, V., Weeks, O., et al. (2010). Alzheimer's beta-amyloid peptide blocks vascular endothelial growth factor mediated signaling via direct interaction with VEGFR-2. *J. Neurochem.* 112, 66–76. doi: 10.1111/j.1471-4159.2009.06426.x

Pei, J. J., Braak, H., An, W. L., Winblad, B., Cowburn, R. F., Iqbal, K., et al. (2002). Up-regulation of mitogen-activated protein kinases ERK1/2 and MEK1/2 is associated with the progression of neurofibrillary degeneration in Alzheimer's disease. *Brain Res. Mol. Brain Res.* 109, 45–55. doi: 10.1016/S0169-328X(02)00488-6

Peiris-Pages, M., Harper, S. J., Bates, D. O., and Ramani, P. (2010). Balance of pro- versus anti-angiogenic splice isoforms of vascular endothelial growth factor as a regulator of neuroblastoma growth. *J. Pathol.* 222, 138–147. doi: 10.1002/path.2746

Provias, J., and Jeynes, B. (2008). Neurofibrillary tangles and senile plaques in Alzheimer's brains are associated with reduced capillary expression of vascular endothelial growth factor and endothelial nitric oxide synthase. *Curr. Neurovasc. Res.* 5, 199–205. doi: 10.2174/156720208785425729

Salomon-Zimri, S., Glat, M. J., Barhum, Y., Luz, I., Boehm-Cagan, A., Liraz, O., et al. (2016). Reversal of ApoE4-driven Brain pathology by vascular endothelial growth factor treatment. *J. Alzheimers Dis.* 53, 1443–1458. doi: 10.3233/JAD-160182

Saraswat, D., Nehra, S., Chaudhary, K., and Cvs, S. P. (2015). Novel vascular endothelial growth factor blocker improves cellular viability and reduces hypobaric hypoxia-induced vascular leakage and oedema in rat brain. *Clin. Exp. Pharmacol. Physiol.* 42, 475–484. doi: 10.1111/1440-1681.12387

Stine, W. B., Jungbauer, L., Yu, C. J., and Ladu, M. J. (2011). Preparing synthetic a beta in different aggregation states. *Alzheimer's Dis. Frontotemp. Dement.* 670, 13–32. doi: 10.1007/978-1-60761-744-0_2

Storkebaum, E., Lambrechts, D., and Carmeliet, P. (2004). VEGF: once regarded as a specific angiogenic factor, now implicated in neuroprotection. *BioEssays* 26, 943–954. doi: 10.1002/bies.20092

Theofilas, P., Ehrenberg, A. J., Nguy, A., Thackrey, J. M., Dunlop, S., Mejia, M. B., et al. (2018). Probing the correlation of neuronal loss, neurofibrillary tangles, and cell death markers across the Alzheimer's disease Braak stages: a quantitative study in humans. *Neurobiol. Aging* 61, 1–12. doi: 10.1016/j.neurobiolaging.2017.09.007

Thomas, T., Miners, S., and Love, S. (2015). Post-mortem assessment of hypoperfusion of cerebral cortex in Alzheimer's disease and vascular dementia. *Brain* 138, 1059–1069. doi: 10.1093/brain/awv025

Tzelepis, K., De Braekeleer, E., Aspris, D., Barbieri, I., Vijayabaskar, M. S., Liu, W. H., et al. (2018). SRPK1 maintains acute myeloid leukemia through effects on isoform usage of epigenetic regulators including BRD4. *Nat. Commun.* 9:5378. doi: 10.1038/s41467-018-07620-0

Veeranna, T., Kaji, B., Boland, T., Odrljin, P., Mohan, B. S., Basavarajappa, C., et al. (2004). Calpain mediates calcium-induced activation of the erk1,2 MAPK pathway and cytoskeletal phosphorylation in neurons: relevance to Alzheimer's disease. *Am. J. Pathol.* 165, 795–805. doi: 10.1016/S0002-9440(10)63342-1

Wakiya, K., and Shibuya, M. (1999). Okadaic acid stimulates the expression of vascular endothelial growth factor gene. *Biochem. Biophys. Res. Commun.* 265, 584–588. doi: 10.1006/bbrc.1999.1724

Yang, S. P., Bae, D. G., Kang, H. J., Gwag, B. J., Gho, Y. S., and Chae, C. B. (2004). Co-accumulation of vascular endothelial growth factor with beta-amyloid in the brain of patients with Alzheimer's disease. *Neurobiol. Aging* 25, 283–290. doi: 10.1016/S0197-4580(03)00111-8

Zheng, X. L., Xie, Z. H., Zhu, Z. Y., Liu, Z., Wang, Y., Wei, L. F., et al. (2014). Methyllycaconitine alleviates amyloid-beta peptides-induced cytotoxicity in SH-SY5Y cells. *PLoS One* 9:e111536. doi: 10.1371/journal.pone.0111536

Zlokovic, B. V. (2011). Neurovascular pathways to neurodegeneration in Alzheimer's disease and other disorders. *Nat. Rev. Neurosci.* 12, 723–738. doi: 10.1038/nrn3114